# Effects of the Hydrophobicity of Substrate on Inverse Opal Structures of Poly(pyrrole) Fabricated by Colloidal Templating

**Jung Min Lee, Dong Gyu Lee, and Jung Hyun Kim***

*Department of Chemical Engineering, Yonsei University, 134 Shinchon-Dong, Seodaemoon-Gu, Seoul 120-749, Republic of Korea*

**In Woo Cheong**

*Department of Applied Chemistry, Kyungpook National University, 1370 Sankyuk-dong, Buk-gu, Daegu 702-701, Republic of Korea*

*Received July 10, 2007; Revised Manuscript Received October 16, 2007*

ABSTRACT: A colloidal templating method with vapor-phase oxidative polymerization was used to fabricate conducting poly(pyrrole) (Ppy) inverse opal patterns over a wide area. We fabricated 2- and 3-D Ppy inverse opal patterns from two kinds of 2- and 3-D colloidal templates of poly(St/NaSS) latex particle, which were prepared on bare glass and 3-aminopropyl trimethoxysilane (APTMS)-modified glass substrates, respectively. With two different 2-D colloidal templates, different Ppy inverse opal monolayer patterns, i.e., ordered 2-D rings, hexagonal or honeycomb monolayer, were obtained. With 3-D colloidal templates, Ppy inverse opal multilayers were obtained and their time-evolution growths were observed by SEM analysis. Differences in inverse opal structure and volume fraction were elucidated in terms of the array pattern of sacrificial poly(St/NaSS) latex particles and its packing density. Shrinkage of the inverse opal structure, which might be a serious problem in optical and physical properties, was reduced to almost zero with this method. Mechanical and electrical properties of the Ppy inverse opal multilayer films were analyzed by nanoindentation and four-point probe conductivity methods, respectively. It was found that narrow interparticle interstices of colloidal templates led to honeycomblike 2- and 3-D patterns, higher modulus and hardness, and lower electrical conductivity. In contrast, a spacious colloidal pattern resulted in 2-D ring patterns, hexagonal 2- and 3-D patterns, lower modulus and hardness, and higher electrical conductivity.

## Introduction

Recently, novel materials based on two-[1−4] and three-dimensional[5−8] ordered colloidal structures, i.e., inorganic silica and/or organic polymer colloidal crystals, have been invented and widely investigated. In particular, photonic crystals for the visible range have been prepared by the self-assembly technique using polymer colloids of several hundred nanometers in diameter, which are dried and crystallized into a face-centered cubic lattice. In just a few years, the fabrication of porous materials using colloidal crystal templates, namely inverse opal structures, has become a promising alternative in order to realize the full potential of three-dimensional photonic crystals for practical device applications. One approach for creating inverse opal structures is to replicate the structure of these photonic crystals in a durable matrix, i.e., silica ($SiO_2$) or titania ($TiO_2$). The original colloidal particles are subsequently removed, leaving behind a new type of material whose pores preserve valuable optical properties of the colloidal crystal. Many methods such as surfactant-[9,10] or UV-induced[11−13] polymerization, sol−gel hydrolysis,[14] hydrolysis,[15,16] pyrolysis,[17] particle infusion,[18] chemical vapor deposition,[17] electrodeposition,[19] electropolymerization,[20] etc. have been tried to make porous inverse opal materials from a wide variety of precursors or monomers and templates. In these methods, the colloidal crystals serve as templates, with the voids infiltrated by material that solidifies in place without disrupting the order of the crystal.[21]

Among the methods, those for electrochemical ones are very complex to set the experimental equipment for preparing the conducting polymer inverse opals because they need many accessories, such as many electrodes, ITO-coated glass, metal paste, potentiostat, etc. On the other hand, vapor-phase oxidative polymerization provides a simple route that directly allows preparation of the conducting polymer inverse opal patterns over a wide area by controlling the amount of oxidant (i.e., $FeCl_3$) embedded in a colloidal crystal template. The vapor-phase oxidative polymerization method also presents an additional advantage in that reaction conditions (polymerization time, polymerization temperature, a kind of monomer, etc.) can easily be controlled to achieve various morphologies such as ordered 2-D ring patterns, hexagonal or honeycomb monolayer, multilayers with highly porous interconnected pores, and so on. Polymeric materials with ordered microstructures are one of the most important to a range of areas such as the fabrication of optical devices, electronic devices, actuators, sensors, and even polymer-based circuits, etc.[22] Most current techniques (i.e., e-beam lithography and soft lithography) use metallic, semiconductor, or polymeric masks or molds to transfer relief structures into polymeric materials. Lithographical microfabrication techniques such as e-beam lithography can be used to create ordered array patterns or microstructures that are submicrometer in both thickness and diameter. These techniques, however, have the significant limitations of being both expensive and time-consuming due to the multistep procedures. Therefore, the colloidal crystal templating method, which can be fast and inexpensive as the nonlithographical technique, is worth investigating. In fact, this method, which is based on the use of colloidal crystals of sub-micrometer polymer latex or silica spheres as a template, is in the limelight as an attractive alternative. In recent years, there have been numerous studies

* To whom correspondence should be addressed. Tel: +82 2 2123 7633. Fax: +82 2 312 0305. E-mail: jayhkim@yonsei.ac.kr.

10.1021/ma071523v CCC: $37.00 
Published on Web 11/30/2007

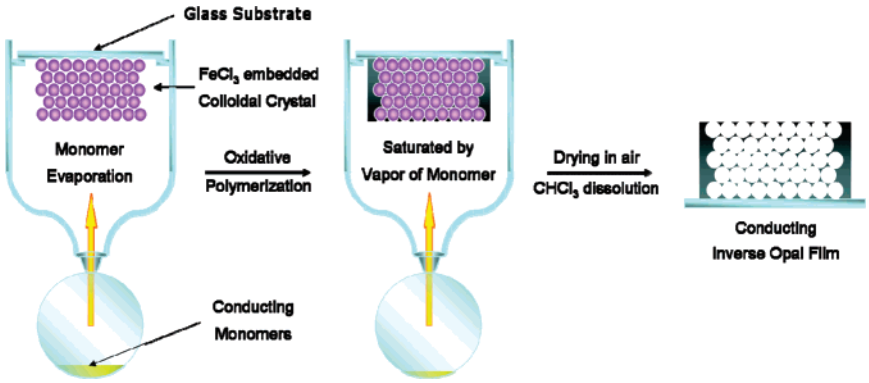


**Figure 1.** Fabrication of Ppy inverse opal by vapor-phase oxidative polymerization of pyrrole with a template of poly(St/NaSS) colloid crystal. The resulting Ppy layer was dried under air prior to exposure to $CHCl_3$ to remove the colloidal template.

on the growth conditions of colloidal crystals, which are made by the convective drying method;[23] however, information on the growth mechanism of the conducting inverse opal film from the colloidal crystals is very limited.[20] The growth mechanism of vapor-phase oxidative polymerization of the conducting inverse opal structure in both the monolayer and multilayer has not been reported.

In this study, we fabricated 2- and 3-D poly(pyrrole) (Ppy) inverse opal patterns from two kinds of colloidal templates, which were prepared on bare glass and 3-aminopropyl trimethoxysilane (APTMS)-modified glass substrates, respectively. The inverse opal structure was made by using oxidative polymerization of vaporizing pyrrole monomer. The colloidal templates were prepared using monodisperse and submicrometer-sized poly(styrene/sodium *p*-styrene sulfonate) (poly(St/NaSS)) particles. Direct observation of the growth of 2- and 3-D Ppy inverse opal films was carried out by controlling the polymerization time.

## Experimental Section

**Materials.** Styrene monomer (St, Junsei, Japan) was purchased and purified using an inhibitor remover column (Aldrich, USA). The purified monomer was kept at −5 °C until use. Sodium *p*-styrene sulfonate (NaSS, Aldrich, USA) was purchased and used as received. Potassium persulfate (KPS, Junsei, Japan) was recrystallized with methanol, dried in a vacuum oven, and kept at −5 °C until use. Sodium bicarbonate ($NaHCO_3$), 3-aminopropyl trimethoxysilane (APTMS), and anhydrous methanol were chosen as analytical grades and used without further purification. Pyrrole monomer (99% purity, Acros Organics, USA) was refrigerated at −5 °C until use. Anhydrous ferric chloride ($FeCl_3$, Kanto Chemical, Japan) and chloroform ($CHCl_3$, 99% purity, Samchun Chemical, Korea) were obtained and used as received. $FeCl_3$ was used as an oxidant. They were all analytical grade and used without further purification. Double-distilled and deionized (DDI) water was used throughout the experiment.

**Preparation of 2- and 3-D Colloid Crystal Templates.** For 2- and 3-D colloid crystals as a template, a natural convection drying method was applied. Purified latex (0.02 wt % solid) was deposited on a stainless steel (40 mm × 40 mm × 2 mm) plate with a circular tapered hole (diameter = 15 mm, taper angle = 60°) in its center, and the cell was allowed to dry in the incubator to form colloid crystals at 20 °C. In order to prepare colloid crystal templates on the hydrophobic substrates, we modified the bare glass substrates with APTMS and applied the natural convection drying method under the same conditions on the bare glass substrate.[24] Monodisperse poly(St/NaSS) latex particles used for colloidal crystal templates were prepared by emulsifier-free emulsion polymerization.[25,26] The number-average particle size ($D_n$) and the polydispersity index ($D_w/D_n$) were 235 nm and 1.007, respectively. The surface charge density ($\sigma$) was 38 $\mu$C cm$^{-2}$.

**Preparation of 2- and 3-D Ppy Inverse Opals.** Vapor-phase oxidative polymerization was carried out with the colloidal template at 40 °C for an appropriate time (monolayer growth: 10 s to 60 min, multilayer growth: from 10 to 180 min). Figure 1 shows a schematic for the fabrication of a conducting Ppy inverse opal structure, which was obtained by the vapor-phase oxidative polymerization of a pyrrole monomer within the interstices of a colloid crystal. 2- and 3-D colloid crystals of poly(St/NaSS) particles were first prepared by a natural convection drying method. The crystals of mono- and multilayer in a wide area of 150 mm$^2$ were obtained, and then the crevices of colloidal crystal template were infiltrated with a $FeCl_3$ aqueous solution ($6.2 \times 10^{-4}$ mol, 0.1 g) by using a spraying method. The crystal template was dried to remove any residual water at room temperature for 1 day. After drying, vapor-phase oxidative polymerizations of pyrrole were carried out with $1.5 \times 10^{-3}$ mol of pyrrole monomer. For investigation of the time-evolution growth of inverse opal structure, the resulting Ppy films were sampled and exposed to a chloroform ($CHCl_3$) solution for 10 h to remove the template.

**Characterization.** Array patterns and inverse opal patterns were observed by using a field-emission scanning electron microscope (FE-SEM, JSM-6500F, JEOL Co., Japan). The ordered 2-D array patterns of Ppy were obtained by atomic force microscope (AFM, Digital Instruments IVa), and all AFM images were obtained by tapping (noncontact) mode under ambient conditions. A nanoindenter (MTS XP System, MTS Systems Corp., USA) was used to measure the mechanical properties of Ppy inverse opal films at 25 °C. In this experiment, a diamond Berkovich-type indenter tip was forced onto the sample being studied. The indentation depth is related to the area of contact between the indenter and the sample being tested. Multiple (five times) indentations were made at different locations on the film surface at a fixed applied load (max load = 6 mN). The load-displacement curves were recorded, from which the effective hardness and modulus values could be calculated. The electrical conductivities of two kinds of Ppy inverse opal films were determined using a standard four-point probe technique (RT-70/RG-5 four-point probe system, Napson Co., Japan) at room temperature. Sheet resistivity of the Ppy inverse opal monolayer films on each substrate was measured and converted into electrical conductivity (S cm$^{-1}$). The resistivity measurement of specimen layers, such as thin films, is affected by the size and thickness of the specimen to the probe pin spacing, the configuration of the specimen and the measuring position. Sheet resistivity can be found by the following equation:

$$\rho = 4.532 \frac{V}{I} tC_{cf} \ (\Omega \cdot \mathrm{cm}) \qquad (1)$$

where $t$ is the thickness of the specimen, and $C_{cf}$ is the correction factor for the size and configuration of the specimen, and the measuring position.

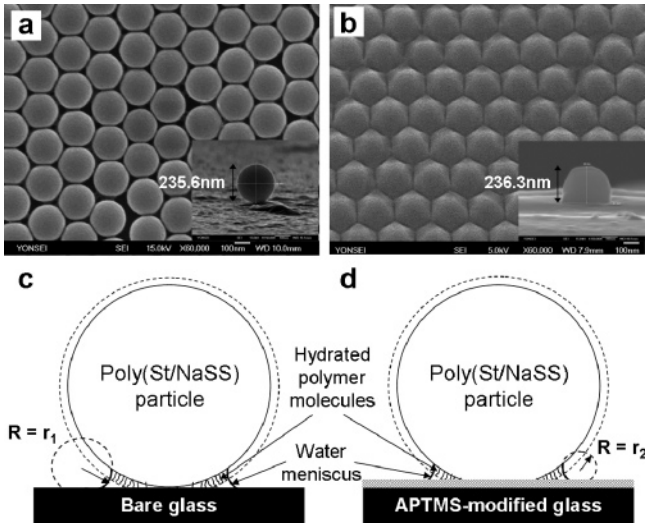


**Figure 2.** Top-view SEM image of a poly(St/NaSS) particle monolayer prepared on the bare glass (a), and APTMS-modified glass (b) substrates at 20 °C. Schematic of the formation of water meniscus between the hydrated poly(St/NaSS) particle and different substrates, (c) bare glass and (d) APTMS-modified glass substrates, during the drying of water.

## Results and Discussion

**Formation of Poly(St/NaSS) Colloidal Templates.** The FE-SEM micrographs in Figure 2a and b show the top view of a poly(St/NaSS) particle monolayer, i.e., 2-D colloid crystal templates, prepared on the bare glass (a) and APTMS-modified glass (b) substrates at 20 °C. The crystal lattice of the bare glass substrate showed an irregular interparticle spacing; however, a very regular hexagonal lattice and adhesional particle deformation were found on the APTMS-modified glass sample. This adhesional particle deformation resulted from the surface modification of the substrates with APTMS.[24] The insets in Figure 2a and b (85° tilted views) show individual poly(St/NaSS) particles and provide further evidence on the adhesional deformation of the individual poly(St/NaSS) particle on the APTMS-modified glass substrate. As shown in Figure 2a, the individual particle lies on the bare glass substrate without any discernible deformation. On the other hand, the particles in Figure 2b adhered to the surface of the APTMS-modified glass substrate were clearly deformed.

Figure 2c and d shows a schematic for the formation of water meniscus between the hydrated poly(St/NaSS) particle and different substrates, (c) bare glass and (d) APTMS-modified glass substrates. Particle deformation was achieved during the natural convective drying due to the large capillary force at the water meniscus, which was formed between the hydrated poly(St/NaSS) molecules on the surface of the particle and the APTMS-modified glass substrate. If a particle weighed on the 'grasslike' soft substrate, the contact surface of the substrate deformed to close up the surface of the particle. The APTMS coating seemed to offer a softer substrate surface, like "grass", than the bare glass substrate, thus providing a greater contact area of poly(St/NaSS) particles with the APTMS coating. As a result of the greater contact area, the interstice between the particle and the APTMS surface was reduced. This reduced interstice provides a stronger capillary force since capillary pressure is inversely proportional to the interstice size ($r_1$ and $r_2$) between the particle surface and substrate according to the Young−Laplace equation ($\Delta P = 2\gamma/R$, where $R = r_1$, $r_2$, and $r_1 > r_2$) for spherical surfaces. This larger capillary force at the water meniscus in the interstices caused the adhesional deformation of the hydrated particles during natural convection drying.

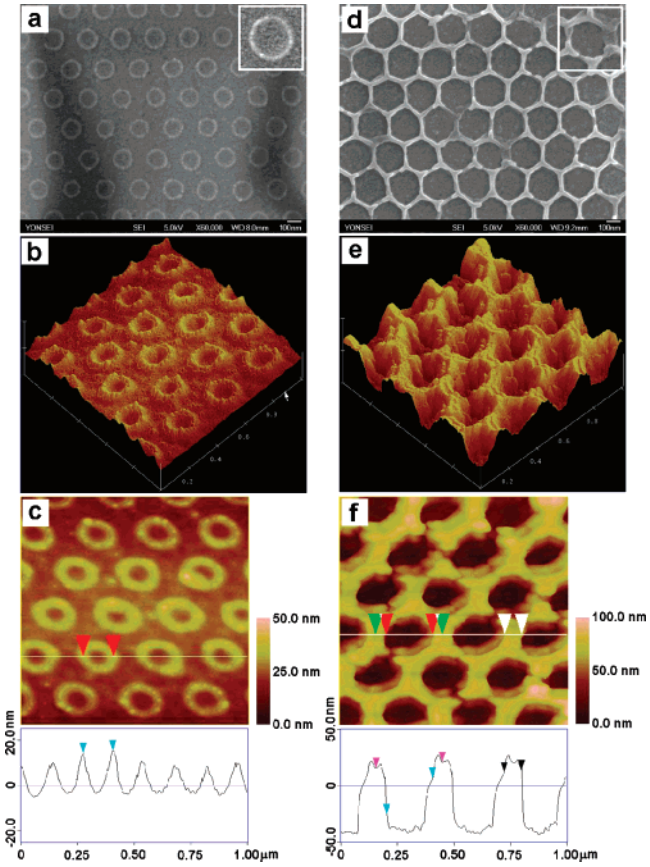


**Figure 3.** SEM image (a) of Ppy 2-D array was captured at 10 min after the beginning of vapor-phase oxidative polymerization at 40 °C. The 2-D ring pattern of Ppy inverse opal was obtained with the poly(St/NaSS) colloidal template fabricated on the bare glass substrate. The corresponding surface plot AFM image (b) and top-view AFM image with a tracing of the *z*-axis profiles (c) were presented. The SEM image (d) of Ppy 2-D array was captured at 90 s after the polymerization. The 2-D honeycomb pattern of Ppy inverse opal was obtained with the colloidal template fabricated on the APTMS-modified glass substrate. The corresponding surface plot AFM image (e) and top-view AFM image with a tracing of the *z*-axis profiles (f) were presented.

After all, the adhesional deformation of the particles resulted from the surface modification of the substrates, and provides an important basis for the different morphologies of the Ppy inverse opal films between on bare glass and on APTMS-modified glass substrates.

**Formation of 2-D Ppy Patterns.** Figure 3a and d indicates the SEM images of different 2-D array patterns of Ppy inverse opal that were fabricated from the two different poly(St/NaSS) colloidal templates. Detailed reaction and analytic conditions are described in the figure caption. As shown in Figure 3a, the ordered 2-D ring patterns were obtained with the colloidal template shown in Figure 2a. On the other hand, the 2-D honeycomb pattern in Figure 3b was obtained with the template shown in Figure 2b. As seen in Figure 3a, submicrometer-sized rings of Ppy were formed on the bare glass substrate with 2-D poly(St/NaSS) colloidal array. The Ppy rings were formed in the smallest interstice at the contact point between the bare glass substrate and the particles, where pyrrole vapor was easily condensed to be polymerized. A detailed description for the growth of Ppy ring was presented in Figure 4. The center-to-center spacing of Ppy ring pattern is consistent with the lattice constant of the sacrificial 2-D poly(St/NaSS) latex colloid (~235 nm) array. AFM analysis was performed in height mode and shown in Figure 3b and 3c. The Ppy rings were ~125 nm in

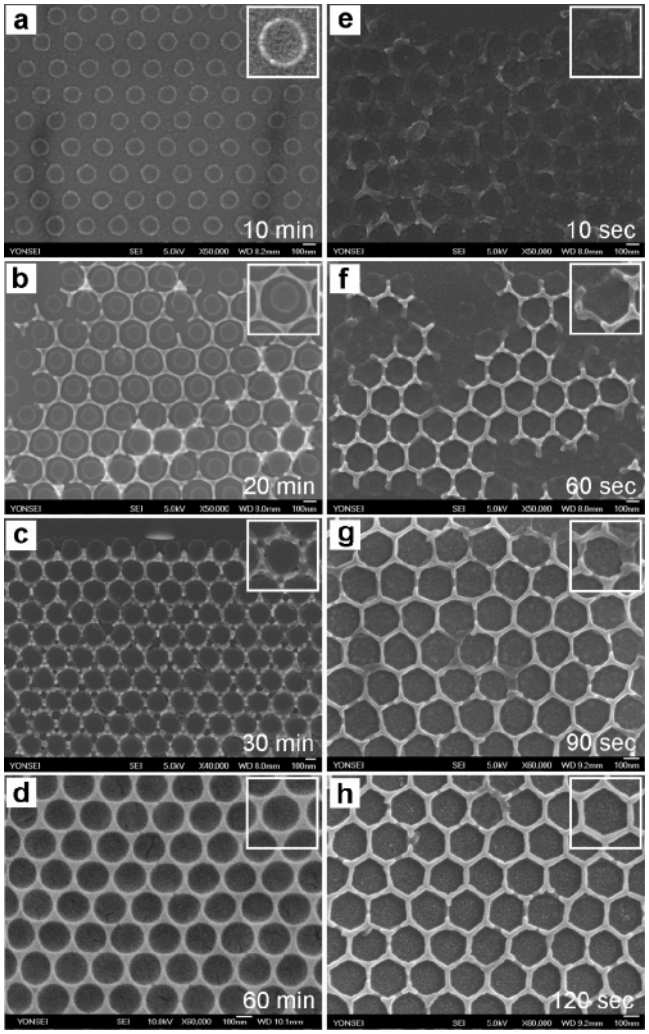


**Figure 4.** Time-evolution SEM images of 2-D Ppy inverse opal monolayers on different colloidal templates; 2-D array of poly(St/NaSS) latex particles on the bare glass (a−d) and the same particle array on the APTMS-modified glass substrates (e−h). The time in each SEM micrograph indicates the polymerization time of pyrrole monomer.

diameter, 20−25 nm in height, and 100 nm in width, as seen in the top-view AFM image and tracing of the *z*-axis profiles.

In contrast, a honeycomb 2-D pattern of Ppy was observed on the APTMS-modified glass substrate with 2-D poly(St/NaSS) colloidal array. This different pattern is believed to originate from the particle deformation on the APTMS-modified glass substrate. As shown in Figure 2b, there was not enough spacing between particles and surface of the substrate due to the adhesional deformation of the particles. In the colloidal template of the APTMS-modified glass substrate, the lower hemisphere of particle was deformed by the larger capillary force at the water meniscus in the interstices between the particle and the APTMS surface during the formation of the monolayer. The interstice spacings between the particles and the APTMS-modified glass substrate became so small in consequence of the adhesional deformation of the hydrated particles. The spacing of periodic pattern was ca. 210 nm, which was smaller than the size of sacrificial poly(St/NaSS) latex particle (∼235 nm). The results were consistent with the AFM data for the interparticle distance (209 nm) of the same latex particles shown in our previous work.[24] As shown in Figure 3f, the wall of honeycomblike Ppy pattern were approximately 22 ± 2 nm in thickness and 59 ± 2 nm in height, obtained from the tracing of the *z*-axis profiles of the pore array.

**Growth of 2-D Ppy Inverse Opal Monolayers.** Figure 4 shows the time-evolution SEM images of 2-D Ppy inverse opal monolayer on the different colloidal templates, i.e., the bare (a−d) and APTMS-modified (e−h) glass substrates (see Figure 2). Different time scales were applied due to the different interstice volumes between two colloidal templates. With the SEM images, one can see that the 2-D array of poly(St/NaSS) particles can be used as a good template to fabricate hexagonal (Figure 4d) or honeycomblike (Figure 4h) inverse opal patterns of periodic structure.

A growth mechanism of 2-D Ppy patterns is as follows. When pyrrole was heated, it would be evaporated and then condensed at the contact regions between the particle and the substrate (or between the particles). The condensed pyrrole was instantly polymerized by pre-existing $FeCl_3$. In the case of the colloidal template with the bare glass substrate (see Figure 2a), the polymerization proceeded to the interstices between the substrate and the monolayer of particles along the lower ridge of given particles. Therefore, the ring patterns of Ppy were left after the removal of the template (Figure 4a). After 20 min of polymerization, a thin reticulate Ppy layer was formed at the interstice between the particles and this layer came down on the substrate after removal of the template (Figure 4b). Depending on the interstice size, this monolayer may be simultaneously formed with the ring formation or subsequently formed to the ring formation. As the evaporation and polymerization of pyrrole proceeded, both Ppy polymer layers formed from the ring and the interparticle regions keep growing and fill the vacant vicinities between the glass substrate and particles along the lower ridges of the hemispheres of the particles. Eventually, the two Ppy layers are interconnected and the boundary of ring pattern disappears (Figure 4c). At the same time, this reticulate Ppy layer at the interparticle regions grows in both vertical directions. Therefore, the center of triangular region among three particles could be vacant (Figure 4d), while the three corners seemed to be firm. Since the polymerization proceeded to the center of a tetrahedral (i.e., the triangle) interstice, the central space might not be filled with Ppy polymers or might be easily removed during the removal of colloidal template. As Ppy grew, the vacant spaces between the glass substrate and lower hemispheres of given particles, as well as the tetrahedral interstices, were filled up completely. After 60 min, a hexagonal inverse opal monolayer of Ppy was formed, as seen in Figure 4d.

In the case of the colloidal template with APTMS-modified glass substrate (see Figure 2b), traces of the honeycomblike pattern of Ppy were found (Figure 4e). As shown in Figure 4e−h, a rigid and firm honeycomb Ppy layer was formed completely within 2 min, since pyrrole vapor was easily condensed to be polymerized in the narrow interstices between the deformed particles. In contrast to the reticular Ppy monolayer on the bare glass substrate (Figure 4b), the honeycomb Ppy structure grew in one vertical direction from the particle−particle−substrate contact line. The inset in Figure 4h indicates the repeating unit of the honeycomblike 2-D Ppy inverse opal, which was quite different from that of the 2-D pattern on the bare glass substrate (Figure 4d vs Figure 4h).

Figure 5 suggests a necessary condition to form 2-D hexagonal structure of Ppy inverse opal on the bare glass substrate. One can see a 1-D array of Ppy rings near the border of hexagonal Ppy monolayer in Figure 5a. Imaginary poly(St/NaSS) particles, which were initially deposited on the bare glass substrate, can be drawn as shown in Figure 5b. A separated boundary of the 2-D Ppy layer was induced by the parallel line

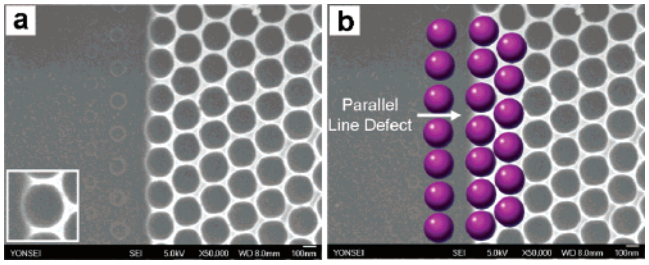


**Figure 5.** SEM image of 2-D Ppy inverse opal monolayer (a) captured at 60 min after initiation and the same image with imaginary poly(St/NaSS) latex particles (b). The arrow indicates a line defect in the 2-D particle array on the bare glass substrate.

defect of the colloid array used as a template. Due to the line defect, spacing between the adjacent particles was too far for pyrrole vapor to be condensed and polymerized as seen in Figure 5b, even though $FeCl_3$ was impregnated all over the surface of substrate. Therefore, it can be concluded that a formation of 2-D Ppy monolayer significantly depends on the interparticle distance, since the volume of the interstice originated from the template is too large for a pyrrole monomer to be condensed. As a result, only ring patterns were formed at the sparsely arrayed particles.

**Growth of 3-D Ppy Inverse Opal Multilayers.** Figure 6 shows the time-evolution SEM images of 3-D Ppy inverse opal multilayer prepared with different colloidal templates. For Figure 6a−d, Ppy inverse opals were fabricated with the template of 3-D poly(St/NaSS) array prepared on the bare glass substrate. These multilayers were captured by FE-SEM at a time interval of 30 min in order to investigate development of growing Ppy structure as the polymerization of pyrrole proceeds. The volume fraction of the colloidal template was measured as 0.74.[24] As shown in Figure 6a−d, a high-quality Ppy inverse opal multilayer with well-defined pore structures was successfully fabricated. As shown in Figure 6a, concave and tetrahedral Ppy wall structures having a triangular void were formed at the triangular contact point between bottom and top layer of particles. The polymerization was initiated at the smallest contact points between $(n-1)$th and $n$th layers of particles and growing Ppy layer started to fill up the tetrahedral interstice between the $(n-1)$th and $n$th layers of particles, as seen in Figure 6a and b. As Ppy climbed over the upper hemispheres of given particles, the walls of Ppy inverse opals became thicker, as seen in Figure 6c and d. The insets in Figure 6 show growing tetrahedral Ppy units by vapor-phase oxidative polymerization of pyrrole. The Ppy volume fraction ($\phi_p$) was measured as $\phi_p = 0.26$.[24]

For Figure 6e−h, the colloidal template used for Ppy inverse opal was 3-D poly(St/NaSS) array prepared on the APTMS-modified glass substrate. Due to the higher packing density (~0.80) of poly(St/NaSS) particle array on the APTMS-modified glass substrate,[24] SEM images were captured with a time interval of 10 min. In this case, growing Ppy immediately climbed up the upper hemispheres of densely packed particles within 10 min and then covered the surfaces of sacrificial poly(St/NaSS) particles (Figure 6e and f). Thus, the tetrahedral interstices between the poly(St/NaSS) particles are seemingly void. The concave tetrahedral structure originated from the higher packing density arising from adhesional deformation of poly(St/NaSS) latex particle. Due to the higher packing density of the poly(St/NaSS) particle array, the volume of the interstice was smaller. Therefore, Ppy grew fast in the vertical direction to cover the upper hemisphere of the poly(St/NaSS) particles. After 30 min, a half of the upper hemisphere was irregularly

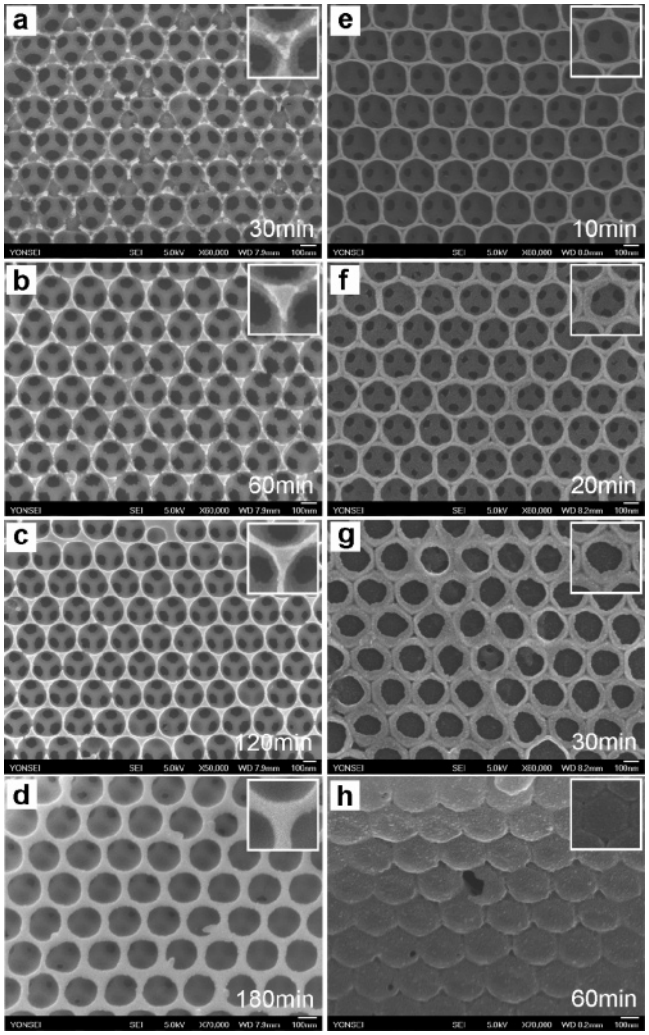


**Figure 6.** Time-evolution SEM images of 3-D Ppy inverse opal multilayers on different colloidal templates; 3-D array of poly(St/NaSS) latex particles on the bare glass (a−d) and the same particle array on the APTMS-modified glass substrates (e−h). The time in each SEM micrograph indicates the polymerization time of pyrrole monomer.

**Table 1. Nanoindentation Data for 3-D Ppy Inverse Opal Films on Different Colloidal Templates Prepared on (a) Bare Glass and (b) APTMS-Modified Glass Substrates at 25 °C**

| values[a] | a | b |
|---|---|---|
| load (mN)[b] | 1.2 ± 0.4 | 2.6 ± 1.0 |
| penetration depth (nm) | 258.2 ± 15.2 | 232.7 ± 8.6 |
| modulus (GPa) | 40.3 ± 5.9 | 48.4 ± 4.3 |
| hardness (GPa) | 0.7 ± 0.4 | 2.3 ± 0.8 |

[a] Each value is the average value from five measurements. [b] The applied max load was 6 mN.

covered, as shown in Figure 6g. Eventually, the upper hemispheres of the latex particles were covered up completely (Figure 6h). Ppy volume fraction of the inverse opal structure was measured as $\phi_p = 0.20$.[24]

**Pore Dimension of 3-D Ppy Inverse Opal Multilayers.** Figure 6a−d indicates a hexagonally well-ordered pore structure of (111) fcc lattice. From Figure 6a, the average channel size at the contact region between the particles was 96 ± 4 nm and the average pore size was 234 ± 7 nm. As Ppy grew, both the average channel and pore sizes became smaller, as seen in Figure 6c and d, while the average center-to-center distance between the pores remained constant, ~241 ± 6 nm. This value corresponds to the average center-to-center distance between sacrificial poly(St/NaSS) latexes (245 ± 8 nm). For the APTMS-

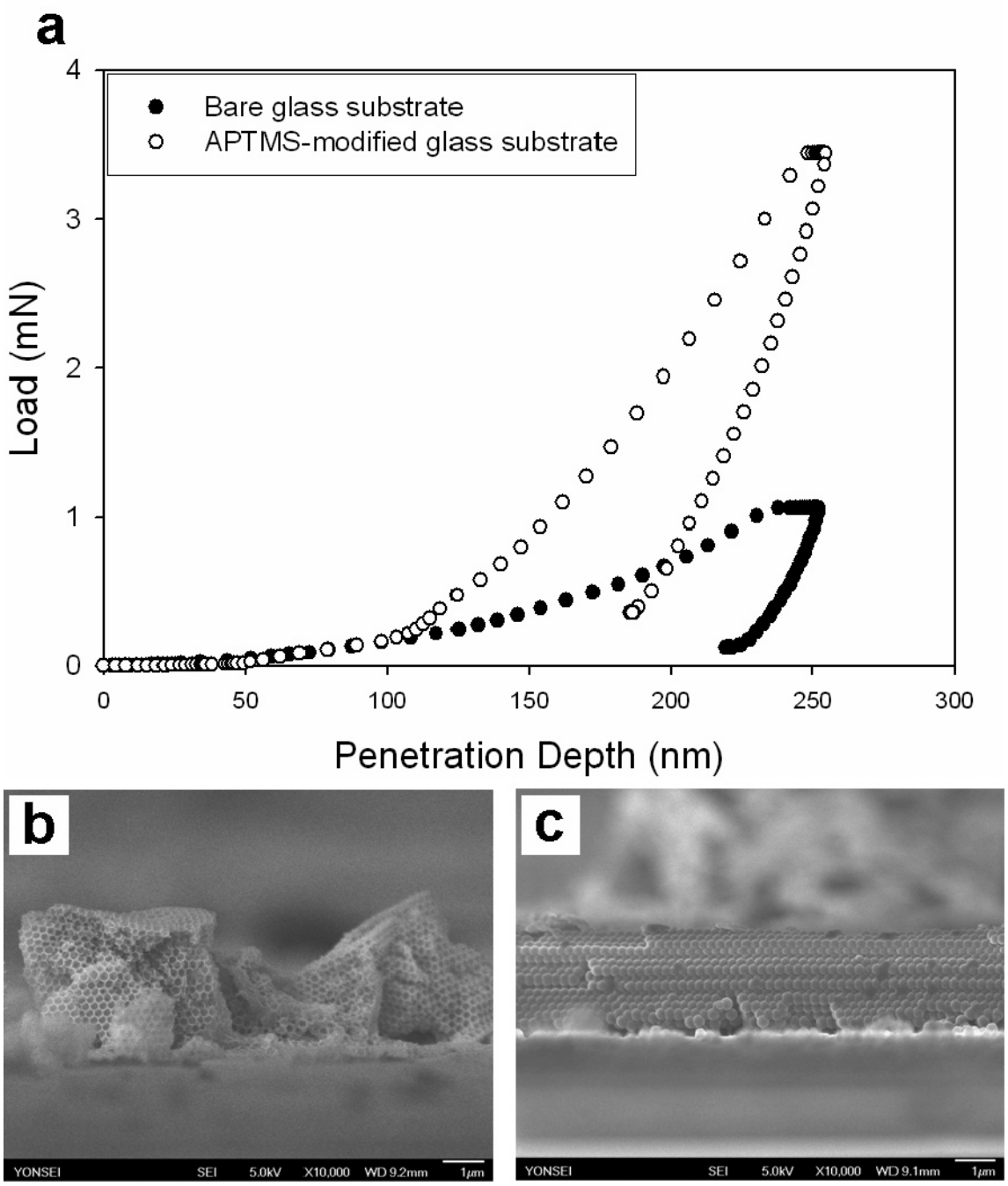


**Figure 7.** Nanoindentation curves of Ppy inverse opal multilayers (a). The SEM images (b and c) are the 90° tilted SEM images of Ppy inverse opal films prepared on the bare glass substrate (●) and APTMS-modified glass substrate (○), respectively, which were tested in nanoindentation analysis. Morphology of Ppy inverse opal films on the APTMS-modified template seems like that of colloidal particle arrays.

modified glass substrate, the average channel size was 68 ± 2 nm and the average pore size was 204 ± 3 nm (Figure 6e). As Ppy grew, both the average channel and pore sizes also became smaller, as seen in Figure 6f and g, while the average center-to-center distance between the pores remained constant, ~213 ± 5 nm, which was in accordance with the average center-to-center distance of the sacrificial deformed poly(St/NaSS) particles (209 ± 1 nm). In this case, the average distance slightly increased, but it might be an error of measurement.

For inverse opal fabrications, it was reported that sol−gel process of metal alkoxides invariably resulted in a linear shrinkage of 25−30%.[27] On the other hand, electropolymerization of conducting polymers resulted in a linear shrinkage

**Table 2. Electrical Conductivity Data for 2-D Ppy Inverse Opal Monolayer Fabricated with the Colloidal Templates (a) with Bare Glass and (b) APTMS-Modified Glass Substrates**

| values | a | b |
|---|---|---|
| sheet resistance[a] (Ω/□) | $0.761 \times 10^4 \pm 0.02$ | $2.054 \times 10^4 \pm 0.05$ |
| specific resistance($\rho$)[b] (Ω·cm) | 0.18 | 0.48 |
| conductivity[c] ($S\ cm^{-1}$) | 5.6 | 2.1 |

[a] Sheet resistances of Ppy inverse opal monolayer films were determined using standard four-point probe techniques at 20 °C. [b] The thickness of Ppy inverse opal monolayers was 235 nm. [c] Conductivity = 1/Specific resistance; the applied current and voltage were 10 μA and 100 mV, respectively.

**Table 3. Electrical Conductivity Data for Ppy with Various Morphologies**

| research group | structure | synthetic method | conductivity (S $cm^{-1}$) | ref |
|---|---|---|---|---|
| our results | inverse opal films | vapor-phase oxidative polymerization | 5.6[a], 2.1[b] | |
| Pei et al. | bulk films | electro-polymerization | $1.0 \times 10^{-2}$−$1.0 \times 10^{1}$ | 28 |
| Lee et al. | bulk films | chemical oxidative polymerization | $1.0 \times 10^{-7}$−$1.0 \times 10^{-1}$ | 29 |
| Ishizu et al. | colloidal particles | chemical oxidative polymerization via emulsion method | $1.0 \times 10^{-5}$−$1.0 \times 10^{-1}$ | 30 |
| Armes et al. | colloidal particles | chemical oxidative polymerization via dispersion method | 0.8−6.2, 3.0−28.0 | 31, 32 |
| Ruckenstein et al. | powders | chemical oxidative polymerization via inverted emulsion method | 9.8−34.2 | 33 |
| Jang et al. | nanotubes | chemical oxidative polymerization via reverse emulsion method | 24.0−33.0 | 34 |

[a] Ppy inverse opal monolayer fabricated with the colloidal template of bare glass substrate. [b] Ppy inverse opal monolayer fabricated with the colloidal template of APTMS-modified glass substrate.

of 14 ± 1%,[20] which is similar to the shrinkage theoretically expected assuming isotropic shrinkage of the sample (∼14%).[18] With a nanochemical technique in the wet state,[27] a linear shrinkage of ∼5% was reported. This value is 5−6 times less than that obtained for inverse opals fabricated from metal alkoxide precursors using sol−gel techniques.[27] Despite the progress achieved in these studies, the substantial shrinkage of the inverse opals remained as an unsolved problem. However, there was no substantial shrinkage at all in our samples. For the bare glass template, the percentage shrinkage was 1.6%, and this value seems to be negligible, as compared with those of previously reported. Generally, a monomer in the liquid phase undergoes shrinkage during the polymerization. In our case, however, pyrrole vapor is condensed to fill the voids of colloidal template and instantly polymerized, which overcomes the limited isotropic shrinkage value (∼14%) of the infiltration of colloidal nanoparticles into colloidal crystals.[18]

**Nanoindentation Analysis of 3-D Ppy Inverse Opal Multilayers.** Mechanical properties of two 3-D Ppy inverse opal films were measured using nanoindentation behavior. The average values in penetration depth, modulus, and hardness of two films are summarized in Table 1, and their representative load-displacement curves of the films are illustrated with their SEM images in Figure 7. It was observed that there is no substantial difference in the two load−displacement curves of the different glass substrates, which were not shown in this paper. However, the load of Ppy inverse opal films on the APTMS-modified glass substrate (Figure 7c) was higher than that on the bare glass substrate (Figure 7b) at a constant penetration depth above 100 nm, as seen in Figure 7a. Above 100 nm (similar to the initial radius of sacrificial poly(St/NaSS) particles), the load of the films (○) on the APTMS-modified glass substrate increased sharply. As seen in Figure 7c (or Figure 6h), the exterior of Ppy inverse opal structure was covered with Ppy, i.e., Ppy shell. This shell might be dented with ease when load is applied only if the Ppy shell would be flexible.

As given in Table 1, penetration depths (232.7 ± 8.6 vs 258.2 ± 15.2 nm) were similar, but the applied load, hardness, and modulus were significantly different. In the case of Ppy with the template of APTMS-modified glass substrate, both hardness and modulus were higher than those of bare glass substrate. This result can be explained by the Ppy wall structure of APTMS-modified glass substrate sample. A denser Ppy wall structure as mentioned above can effectively decentralize loading force in spite of the low volume fraction of Ppy in the inverse opal structure.

**Electrical Conductivity of 2-D Ppy Inverse Opal Monolayers.** Electrical resistance and conductivity data of 2-D Ppy inverse opal monolayer films fabricated on the different templates were given in Table 2. The conductivity (2.1 S $cm^{-1}$, with APTMS-modified glass substrate) of the Ppy film was 2.5 times lower than that (5.6 S $cm^{-1}$, with bare glass substrate) of the Ppy film at the same measuring conditions. The interstice spacing, filled with Ppy, of the poly(St/NaSS) particles template with APTMS substrate was much narrower than that with bare glass substrate in consequence of the adhesional deformation of the particles. Thus, the amount of Ppy in the templates was smaller than that with bare glass substrate and resulted in the intrinsically low conductivity. Recently, electrical properties of various conducting Ppy structures (i.e., bulk film, colloidal particles, powder, etc.) have been reported. We listed the values of electrical conductivity for various Ppy with different structures in Table 3. In the case of bulk structures, conductivities of the Ppy films with electropolymerization were in the range $1.0 \times 10^{-2}$−$1.0 \times 10^{1}$ S $cm^{-1}$,[28] while conductivities of the Ppy films with chemical oxidative polymerization ($1.0 \times 10^{-7}$−$1.0 \times 10^{-1}$ S $cm^{-1}$)[29] were much lower than those with electropolymerization. Conductivities of the Ppy colloidal particles prepared by emulsion and dispersion methods were in the range $10^{-5}$−$10^{-1}$ [30] and 0.8−28.0 S $cm^{-1}$,[31,32] respectively, depending on the amount of dopant. In the case of powder form, conductivity of the Ppy powders prepared by using inverted emulsions was in the range of 9.8−34.2 S $cm^{-1}$.[33] In recent years, it also has been reported that Ppy nanotubes were readily fabricated through chemical oxidative polymerization in AOT reverse (water-in-oil) emulsions. Its conductivity was in the range 24.0−33.0 S $cm^{-1}$ with increasing wall thickness.[34] Comparing our results with published data, conductivity of the Ppy inverse opal monolayer films was relatively higher than those of bulk films and colloidal particles. This can be explained by the well-ordered Ppy inverse opal structure of good interconnectivity, in spite of low volume fractions (0.20−0.26) of Ppy inverse opal structure.

## Conclusion

We have prepared 2- and 3-D colloidal templates of poly(St/NaSS) latex particles with different interstice size and lattice structures by controlling the hydrophobicity of glass substrates. With these colloidal templates, 2- and 3-D Ppy inverse opal patterns were fabricated via vapor-phase oxidative polymerization. The Ppy inverse opal patterns showed different morphology and volume fraction depending on the interstice size and lattice structure of the colloidal templates, which significantly affected the hardness and modulus of Ppy inverse opal multilayer films. In spite of the low volume fraction of Ppy in the inverse opal structure, an excellent electrical conductivity was obtained. In addition, we have prepared successfully the 3-D inverse opal structure, of which shrinkage was reduced to almost zero through a combination of colloidal templating method and vapor-phase oxidative polymerization. This method can be effectively utilized to prepare mesoporous conductive films with various pore structures and volume factions.

**Acknowledgment.** This work was financially supported by the Ministry of Education and Human Resources Development (MOE), the Ministry of Commerce, Industry and Energy

(MOCIE), and the Ministry of Labor (MOLAB) through the fostering project of the Lab of Excellency and the Ministry of Commerce, Industry, and Energy (MOCIE) through the project of NGNT (No. 10023135-2005-11 and 10024160-2006-12). This work had been supported by the Korea Research Foundation Grant funded by the Korean Government (MOEHRD, R08-2003-000-11116-0).

## References and Notes

(1) Dimitrov, A. S.; Dushkin, C. D.; Yoshimura, H.; Nagayama, K. *Langmuir* **1994**, *10*, 432−440.
(2) Dushkin, C. D.; Lazarov, G. S.; Kotsev, S. N.; Yoshimura, H.; Nagayama, K. *Colloid Polym. Sci.* **1999**, *277*, 914−930.
(3) Maenosono, S.; Dushkin, C. D.; Yamaguchi, Y. *Colloid Polym. Sci.* **1999**, *277*, 993−996.
(4) Nagayama, K. *Phase Transitions* **1993**, *45*, 185−203.
(5) Yablonovitch, E.; Gmitter, T. J. *Phys. Rev. Lett.* **1989**, *63*, 1950−1953.
(6) Ye, Y. H.; Badilescu, S.; Truong, V.-V.; Rochon, P.; Natansohn, A. *Appl. Phys. Lett.* **2001**, *79*, 872−874.
(7) Zeng, F.; Sun, Z.; Wang, C.; Ren, B.; Liu, X.; Tong, Z. *Langmuir* **2002**, *18*, 9116−9120.
(8) Jiang, P.; Hwang, K. S.; Mittleman, D. M.; Bertone, J. F.; Colvin, V. L. *J. Am. Chem. Soc.* **1999**, *121*, 11630−11637.
(9) Velev, O. D.; Jede, T. A.; Lobo, R. F.; Lenhoff, A. M. *Nature* **1997**, *389*, 447−448.
(10) Velev, O. D.; Jede, T. A.; Lobo, R. F.; Lenhoff, A. M. *Chem. Mater.* **1998**, *10*, 3597−3602.
(11) Park, S. H.; Xia, Y. *Adv. Mater.* **1998**, *10*, 1045−1048.
(12) Park, S. H.; Xia, Y. *Chem. Mater.* **1998**, *10*, 1745−1747.
(13) Gates, B.; Yin, Y.; Xia, Y. *Chem. Mater.* **1999**, *11*, 2827−2836.
(14) Imhof, A.; Pine, D. J. *Nature* **1997**, *389*, 948−951.
(15) Holland, B. T.; Blanford, C. F.; Do, T.; Stein, A. *Chem. Mater.* **1999**, *11*, 795−805.
(16) Holland, B. T.; Blanford, C.; Stein, A. *Science* **1998**, *281*, 538−540.
(17) Zakhidov, A. A.; Baughman, R. H.; Iqbal, Z.; Cui, C.; Khayyrullin, I.; Dantas, O.; Marti, J.; Ralchenko, V. G. *Science* **1998**, *282*, 897−901.
(18) Subramanian, G.; Manoharan, V. N.; Thorne, J. D.; Pine, D. J. *Adv. Mater.* **1999**, *11*, 1261−1265.
(19) Yeo, K. H.; Teh, L. K.; Wong, C. C. *J. Cryst. Growth* **2006**, *287*, 180−184.
(20) Cassagneau, T.; Caruso, F. *Adv. Mater.* **2002**, *14*, 34−38.
(21) Velev, O. D.; Kaler, E. W. *Adv. Mater.* **2000**, *12*, 531−534.
(22) Braun, P. V.; Wiltzius, P. *Nature* **1999**, *402*, 603−604.
(23) Denkov, N.; Velev, O.; Kralchevski, P.; Ivanov, I.; Yoshimura, H.; Nagayama, K. *Langmuir* **1992**, *8*, 3183−3190.
(24) Lee, J. M.; Kim, J. H.; Ho, C. C.; Cheong, I. W. *Polymer* **2007**, *48*, 4804−4813.
(25) Cheong, I. W.; Kim, J. H. *Colloid Polym. Sci.* **1997**, *275*, 736−743.
(26) Cheong, I. W.; Kim, J. H. *Colloids Surf. A* **1999**, *153*, 137−142.
(27) Wang, D.; Caruso, F. *Adv. Mater.* **2001**, *13*, 350−354.
(28) Pei, Q.; Qian, R. *Synth. Met.* **1991**, *45*, 35−48.
(29) Lee, D. H.; Chang, J. A.; Kim, J. K. *J. Mater. Chem.* **2006**, *16*, 4575−4580.
(30) Ishizu, K.; Tanaka, H.; Saito, R.; Maruyama, T.; Yamamoto, T. *Polymer* **1996**, *37*, 863−867.
(31) Armes, S. P.; Miller, J. F.; Vincent, B. *J. Colloid Interface Sci.* **1987**, *118*, 410−416.
(32) Armes, S. P.; Miller, J. F. *Synth. Met.* **1988**, *22*, 385−393.
(33) Ruckenstein, E.; Hong, L. *Synth. Met.* **1994**, *66*, 249−256.
(34) Jang, J.; Yoon, H. *Langmuir* **2005**, *21*, 11484−11489.

MA071523V